

# Enhanced Supersymmetric Corrections to Top-Quark Production at the Tevatron

Jaewan Kim<sup>1</sup>, Jorge L. Lopez<sup>2</sup>, D.V. Nanopoulos<sup>1,3</sup>,  
and Raghavan Rangarajan<sup>1</sup>

<sup>1</sup>Astroparticle Physics Group, Houston Advanced Research Center (HARC)  
The Mitchell Campus, The Woodlands, TX 77381, USA

<sup>2</sup>Department of Physics, Bonner Nuclear Lab, Rice University  
6100 Main Street, Houston, TX 77005, USA

<sup>3</sup>Center for Theoretical Physics, Department of Physics, Texas A&M University  
College Station, TX 77843-4242, USA

## Abstract

We calculate the one-loop supersymmetric electroweak-like and QCD-like corrections to the top-quark pair-production cross section at the Tevatron, including the important effects of non-degenerate top-squarks and left-right top-squark mixing. The largest electroweak-like effects yield a negative shift in the cross section and are enhanced right below the threshold for top-quark decay into top-squark and higgsino-like neutralino, and can be as large as  $-35\%$ . The largest QCD-like effects are positive and are enhanced for light top-squark masses, and can be as large as  $20\%$ . Such shifts greatly exceed the present theoretical uncertainty in the Standard Model prediction, and therefore may be experimentally observable. We also explore the one-loop shifts in scenarios containing light top-squarks and higgsino-like neutralinos that have been recently proposed to explain various apparent experimental anomalies.

E-mail addresses:  
jaewan@diana.tdl.harc.edu  
lopez@physics.rice.edu  
dimitri@phys.tamu.edu  
raghu@diana.tdl.harc.edu

# 1 Introduction

The existence of the top quark has now been firmly established by the CDF and D0 Collaborations at Fermilab [1]. The analysis of over  $100 \text{ pb}^{-1}$  of data by each experiment has allowed a determination of the top-quark mass and pair-production cross section [2]

$$m_t^{\text{CDF}} = 176 \pm 9 \text{ GeV}, \quad \sigma_{t\bar{t}}^{\text{CDF}} = 7.6_{-1.5}^{+1.9} \text{ pb}; \quad (1)$$

$$m_t^{\text{D0}} = 170 \pm 18 \text{ GeV}, \quad \sigma_{t\bar{t}}^{\text{D0}} = 5.2 \pm 1.8 \text{ pb}; \quad (2)$$

to better than  $\sim 5\%$  and  $\sim 20\%$  respectively. The experimental error flags are expected to be further reduced when the data set is fully analyzed. A significant increase in sensitivity will become available once the Main Injector upgrade becomes operational in 1999, with an expected reduction in the top-quark mass uncertainty down to 3.5 (2.0) GeV and in the production cross section down to 11% (6%) with an integrated luminosity of  $\mathcal{L} = 1 (10) \text{ fb}^{-1}$  [3]. On the other hand, the theoretical prediction for the cross section in the Standard Model has become rather precise [4, 5, 6], and is presently known to better than 10% for fixed values of  $m_t$ , *e.g.* [5]

$$\sigma_{t\bar{t}}^{\text{theory}} [170] = 6.48_{-0.48}^{+0.09} \text{ pb}, \quad \sigma_{t\bar{t}}^{\text{theory}} [175] = 5.52_{-0.42}^{+0.07} \text{ pb}. \quad (3)$$

The agreement between theoretical expectations and experimental observations is not tight enough to preclude moderate shifts ( $\sim 2 \text{ pb}$ ) to the production cross section from new physics phenomena. However, greater than 50% shifts in the Standard Model prediction due to new physics may conflict with experimental observations. It is then opportune to investigate how large a shift scenarios for new physics may yield, most interestingly in the case of low-energy supersymmetry.

In this paper we consider the one-loop corrections to the pair-production cross section for top quarks at the Tevatron, including both supersymmetric electroweak-like (loops of charginos and bottom-squarks or neutralinos and top-squarks) and QCD-like (loops of gluinos and squarks) contributions. Our calculation extends and corrects those in the literature [7, 8], identifies the largest contributions and determines under what conditions they may be enhanced, and treats all important and realistic effects (such as top-squark mass non-degeneracy and mixing) in a unified way. We also consider specific scenarios with especially light supersymmetric particles that have been proposed in connection with the  $R_b$  observable [9], an as-yet unexcluded light higgsino window [10], and a possible supersymmetric explanation [11, 12] for the  $ee\gamma\gamma$  event observed by CDF [13]. We stress that light supersymmetric particles that affect the top-quark cross section are also likely to affect its decay width via new supersymmetric channels, and the resulting decrease in  $B(t \rightarrow bW)$  may affect the yield of  $bWbW$  events in a much more significant way than a shift in the underlying production cross section.

This paper is organized as follows. In Sec. 2 we present compact expressions for the results of our analytical calculations for the one-loop supersymmetric electroweak-like and QCD-like corrections and contrast them with existing calculations. In Sec. 3

we present a qualitative and quantitative study of the expected corrections and identify regions in parameter space that entail the largest possible effects. These effects may easily exceed the theoretical uncertainty in the Standard Model prediction for the top-quark cross section, and thus may be disentangled at future Tevatron runs. In Sec. 4 we adapt our general results to study specific models that have been proposed in the literature and that contain especially light supersymmetric particles. Sec. 5 summarizes our conclusions and the Appendix contains some further expressions.

## 2 Analytical results

Top-quark pair-production at a hadron collider proceeds at tree-level via two underlying  $s$ -channel parton processes:  $q\bar{q}$  annihilation (see Fig. 1(a)) and gluon fusion. At the Tevatron the first process dominates (90%) [4], and therefore we neglect the latter in what follows. One-loop corrections to  $q\bar{q} \rightarrow g \rightarrow t\bar{t}$  in the context of low-energy supersymmetry fall into two categories: electroweak-like [7] and QCD-like [8]. The significant electroweak-like vertex and external leg corrections modify the outgoing part of the Feynman diagram via new contributions to the  $gt\bar{t}$  vertex and to the normalization of the top-quark wavefunction that involve loops of top-squarks and neutralinos or bottom-squarks and charginos (see Fig. 2). The QCD-like corrections modify both the incoming and outgoing portions of the diagram in an analogous fashion, but involve loops of gluinos and first-generation-squarks or gluinos and top-squarks (see Fig. 3). There are also (smaller) QCD-like box diagram contributions involving gluinos and squarks (see Fig. 3(i)).

The tree-level  $q\bar{q} \rightarrow t\bar{t}$  parton cross section is given by

$$\hat{\sigma} = \frac{8\pi\alpha_s^2}{9\hat{s}^2} \beta_t \frac{1}{3}(\hat{s} + 2m_t^2) \quad (4)$$

where  $\beta_t = \sqrt{1 - 4m_t^2/\hat{s}}$ , and  $\sqrt{\hat{s}}$  is the usual parton-level center-of-mass energy. The supersymmetric electroweak-like one-loop corrections involving the Higgsino components of the neutralinos and charginos are enhanced by a large top-quark Yukawa coupling as seen below

$$\lambda_t \begin{pmatrix} \hat{t}_L \\ \hat{b}_L \end{pmatrix} \widehat{H}_2 \hat{t}_R \ni \lambda_t \tilde{b}_L \widetilde{H}^\pm t_R, \lambda_t t_L \widetilde{H}_2^0 \tilde{t}_R, \lambda_t \tilde{t}_L \widetilde{H}_2^0 t_R, \quad (5)$$

where the carets represent superfields and the terms on the right-hand side include the Yukawa coupling components of interest. These corrections involve loops of top-squarks and neutralinos or bottom-squarks and charginos and are given by

$$\Delta\hat{\sigma}^{\text{EW}} = \frac{8\pi\alpha_s^2}{9\hat{s}^2} \beta_t \left( \frac{\lambda_t}{4\pi} \right)^2 \left[ \frac{2}{3}(\hat{s} + 2m_t^2)(F_1^n + F_1^c) + 2(F_5^n + F_5^c)m_t\hat{s} \right], \quad (6)$$

where  $\lambda_t = gm_t/(\sqrt{2}M_W \sin\beta)$  is the top-quark Yukawa coupling, and  $\tan\beta = v_2/v_1$  where  $v_1, v_2$  are the Higgs vacuum expectation values that arise in the MSSM. Also,

$F_{1,5}^{n,c}$  are form factors that encode the loop functions and depend on the various mass parameters. The top-squark–neutralino form factors are given by:

$$F_1^n = \sum_{j=1}^4 \left\{ N_{j4} N_{j4}^* \sum_{J=1}^2 \left[ c_{24} + m_t^2 (c_{11} + c_{21}) + \frac{1}{2} B_1 + m_t^2 B_1' \right] (\chi_j^0, \tilde{t}_J, \tilde{t}_J) \right. \\ \left. - \text{Re} (N_{j4} N_{j4}) \sum_{J=1}^2 (-1)^{J+1} \sin(2\theta_t) m_t m_{\chi_j^0} (c_0 + c_{11} + B_0') (\chi_j^0, \tilde{t}_J, \tilde{t}_J) \right\}; \quad (7)$$

$$F_5^n = \sum_{j=1}^4 \left\{ N_{j4} N_{j4}^* \sum_{J=1}^2 \left[ -\frac{1}{2} m_t (c_{11} + c_{21}) \right] (\chi_j^0, \tilde{t}_J, \tilde{t}_J) \right. \\ \left. + \text{Re} (N_{j4} N_{j4}) \sum_{J=1}^2 (-1)^{J+1} \frac{1}{2} \sin(2\theta_t) m_{\chi_j^0} (c_0 + c_{11}) (\chi_j^0, \tilde{t}_J, \tilde{t}_J) \right\}. \quad (8)$$

Here  $N_{j4}$  represents the higgsino admixture of  $\chi_j^0$  ( $\tilde{H}_2^0$  in the notation of Eq. (5) and Ref. [14]), and the  $J = 1, 2$  sum runs over the two top-squark mass eigenstates ( $m_{\tilde{t}_{1,2}}$ ), which are obtained from the  $\tilde{t}_{L,R}$  gauge eigenstates via:  $\tilde{t}_1 = \cos \theta_t \tilde{t}_L + \sin \theta_t \tilde{t}_R$  and  $\tilde{t}_2 = -\sin \theta_t \tilde{t}_L + \cos \theta_t \tilde{t}_R$ . The various  $B$  and  $c$  functions in the above expressions are the well documented Passarino-Veltman functions [15] (adapted to our metric where  $p_i^2 = m_i^2$ ); the  $B$  functions depend on  $(m_t, m_{\chi_j^0}, m_{\tilde{t}_J})$  whereas the  $c$  functions depend on  $(-p_3, p_3 + p_4, m_{\chi_j^0}, m_{\tilde{t}_J}, m_{\tilde{t}_J})$  [as reminded by the superscripts in Eqs. (7,8)], where  $p_3$  and  $p_4$  are the momenta of the outgoing top-quark and anti-top-quark respectively (see Fig. 1(b)). The bottom-squark–chargino form factors are in turn given by

$$F_1^c = \sum_{j=1}^2 V_{j2} V_{j2}^* \sum_{J=1}^2 \left( \frac{\cos^2 \theta_b^{(J=1)}}{\sin^2 \theta_b^{(J=2)}} \right) \left[ c_{24} + m_t^2 (c_{11} + c_{21}) + \frac{1}{2} B_1 + m_t^2 B_1' \right] (\chi_j^\pm, \tilde{b}_J, \tilde{b}_J) \quad (9)$$

$$F_5^c = \sum_{j=1}^2 V_{j2} V_{j2}^* \sum_{J=1}^2 \left( \frac{\cos^2 \theta_b^{(J=1)}}{\sin^2 \theta_b^{(J=2)}} \right) \left[ -\frac{1}{2} m_t (c_{11} + c_{21}) \right] (\chi_j^\pm, \tilde{b}_J, \tilde{b}_J), \quad (10)$$

where  $V_{j2}$  represents the higgsino admixture of  $\chi_j^\pm$ , and for completeness we have allowed a non-vanishing bottom-squark mixing angle such that  $\tilde{b}_1 = \cos \theta_b \tilde{b}_L + \sin \theta_b \tilde{b}_R$  and  $\tilde{b}_2 = -\sin \theta_b \tilde{b}_L + \cos \theta_b \tilde{b}_R$ . The  $J = 1, 2$  sum runs over the two bottom-squark mass eigenstates ( $m_{\tilde{b}_{1,2}}$ ). Note that if  $\theta_b = 0$ , only the left-handed bottom-squark is involved in the loops. In Eqs. (9,10) the  $B$  functions depend on  $(m_t, m_{\chi_j^\pm}, m_{\tilde{b}_J})$  whereas the  $c$  functions depend on  $(-p_3, p_3 + p_4, m_{\chi_j^\pm}, m_{\tilde{b}_J}, m_{\tilde{b}_J})$ .

The functions  $B_1$  and  $c_{24}$  in Eqs. (7,9) contain infinities. We used the modified minimal subtraction scheme and introduced counterterms to eliminate them. Nevertheless, it turns out that the infinities (and the renormalization-scale  $\mu$  dependence) of these two functions cancel each other out in both equations (independently) even without introducing counterterms.

Since the Passarino-Veltman functions can be notoriously difficult to evaluate numerically for certain values of the parameters, we have employed different methods

(all of which agree), in particular using the software package **ff** [16]. Our results for the case of no top- or bottom-squark mixing ( $\theta_t = \theta_b = 0$ ) disagree with those originally published in Ref. [7]. However, these authors have since revised their calculation and their corrected expressions [17] are now in agreement with our results above. Our results for the realistic case of squark mixing ( $\theta_t, \theta_b \neq 0$ ) are new.<sup>1</sup>

In Eqs. (6,7,8,9,10) we have not explicitly exhibited the additional contributions to the  $F_{1,5}^{n,c}$  form factors that arise from the gaugino admixtures of the neutralinos and charginos. These are proportional to the electroweak gauge couplings and are therefore not enhanced by a large top-quark Yukawa coupling. These contributions have been neglected in our present analysis. For completeness, in the Appendix we present analytic expressions for the contributions from all (higgsino and gaugino) admixtures to the vertex and external leg corrections. We have also not exhibited the electroweak-like corrections to the incoming part of the diagram, that involve loops of first-generation squarks and neutralinos or charginos. These corrections are rather small as the relation  $m_q \approx m_{\tilde{q}} + m_\chi$ , that the numerical analysis below shows is required for enhancement, is not satisfied in this case. Furthermore, for higgsino-like neutralinos these contributions are proportional to  $m_q^2$  (*c.f.* Eq. (6)) and are therefore negligible.

The QCD-like corrections involve self-energy, vertex, and box diagrams. In the approximation of neglecting the box diagrams,<sup>2</sup> one can readily obtain the shifts in the total parton-level cross sections and cast them in the same format as the electroweak-like corrections given above. In this form comparison between the two classes of corrections becomes transparent. The QCD-like one-loop correction becomes

$$\Delta\hat{\sigma}^{\text{QCD}} = \frac{8\pi\alpha_s^2}{9\hat{s}^2} \beta_t \left( \frac{\alpha_s}{4\pi} \right) \left[ \frac{2}{3}(\hat{s} + 2m_t^2)(F_1^t + F_1^q) + 2F_5^t m_t \hat{s} \right]. \quad (11)$$

The form factor  $F_1^t$ , which modifies the outgoing part of the diagram is given by

$$\begin{aligned} F_1^t = & \sum_{J=1}^2 \left\{ \left(-\frac{1}{3}\right)[c_{24} + m_t^2(c_{11} + c_{21})]^{(\tilde{g}\tilde{t}_J\tilde{t}_J)} + \left(\frac{4}{3}\right)[B_1 + 2m_t^2 B'_1] \right. \\ & + (-1)^J \sin(2\theta_t) m_t m_{\tilde{g}} \left[\left(\frac{1}{3}\right)(c_0 + c_{11})^{(\tilde{g}\tilde{t}_J\tilde{t}_J)} - \left(\frac{8}{3}\right)B'_0\right] \\ & + \left(\frac{3}{2}\right)\left[-\frac{1}{2} + 2c_{24} + \hat{s}(c_{22} - c_{23}) - m_{\tilde{g}}^2 c_0 - m_t^2(c_0 + 2c_{11} + c_{21}) \right. \\ & \left. \left. - (-1)^J 2 \sin(2\theta_t) m_t m_{\tilde{g}}(c_0 + c_{11})\right]^{(\tilde{t}_J\tilde{g}\tilde{g})} \right\}, \quad (12) \end{aligned}$$

where  $\theta_t$  is the top-squark mixing angle, the  $B$  functions depend on  $(m_t, m_{\tilde{g}}, m_{\tilde{t}_J})$ , and the superscripts (*abb*) indicate that the corresponding  $c$  functions depend on  $(-p_3, p_3 + p_4, m_a, m_b, m_b)$ .

The analogous form factor that modifies the incoming part of the diagram ( $F_1^q$ ) is obtained from  $F_1^t$  by setting  $\tilde{t}_J \rightarrow \tilde{q}_J$ ,  $m_t \rightarrow m_q$ ,  $\theta_t \rightarrow \theta_q$ , and by replacing  $p_3, p_4$

<sup>1</sup>While the present paper was being written up Ref. [18] appeared, which contains a calculation of the  $\theta_t \neq 0$  case, that agrees with our result above in the case of real  $N_{j4}$  values.

<sup>2</sup>Recent calculations of supersymmetric QCD-like corrections to light-quark scattering at the Tevatron indicate that box diagram contributions are indeed small near the threshold region [19].

by  $p_1, p_2$ , the incoming quark and anti-quark momenta. Since  $m_q \approx 0$ , the expression for  $F_1^q$  simplifies considerably. Note the close resemblance between the first two lines in  $F_1^t$  and the expression for  $F_1^n$  in Eq. (7) above, as both form factors originate from analogous diagrams ( $\chi_j^0 \leftrightarrow \tilde{g}$ ); the differences in the coefficients stem from the color factors that appear in the QCD-like diagram. In contrast, the last two lines in  $F_1^t$  correspond to a new diagram (not present in the electroweak-like case) where the gluino couples directly to the gluon and which carries a large color factor (Fig. 3(g)). We also have

$$F_5^t = \sum_{J=1}^2 \left\{ \left( \frac{1}{6} \right) [m_t(c_{11} + c_{21}) - (-1)^J \sin(2\theta_t) m_{\tilde{g}}(c_0 + c_{11})]^{(\tilde{g}\tilde{t}_J\tilde{t}_J)} + \left( \frac{3}{2} \right) [m_t(c_{11} + c_{21}) + (-1)^J \sin(2\theta_t) m_{\tilde{g}}c_{11}]^{(\tilde{t}_J\tilde{g}\tilde{g})} \right\}, \quad (13)$$

where we again note the resemblance (up to the color factor coefficient) between the first term in  $F_5^t$  and its counterpart  $F_5^n$  in Eq. (8). The second term in  $F_5^t$  corresponds to the diagram not present in the electroweak-like case. The analogous form factor  $F_5^q$  (that arises from the incoming part of the diagram) is obtained from  $F_5^t$  by setting  $\tilde{t}_J \rightarrow \tilde{q}_J$ ,  $m_t \rightarrow m_q$ ,  $\theta_t \rightarrow \theta_q$ , by introducing an overall minus sign and by replacing  $p_3, p_4$  by  $p_1, p_2$ , the incoming quark and anti-quark momenta. This contribution is negligible since  $m_q \approx 0$  and because in the MSSM  $\theta_q \propto m_q \approx 0$ . Our results for the supersymmetric QCD-like corrections agree with those presented earlier in Ref. [8], and its erratum [20].

For general neutralino composition there exist box diagrams that mix electroweak-like and QCD-like corrections,<sup>3</sup> with gluinos, squarks, top-squarks, and neutralinos in the loop (see Fig. 4). For the higgsino-like neutralino case that we consider, these diagrams are proportional to the light-quark Yukawa coupling and therefore negligible.

The actual observable cross section is obtained by integrating  $\hat{\sigma} + \Delta\hat{\sigma}$  over the parton distribution functions, *i.e.*,

$$\begin{aligned} \sigma + \Delta\sigma = & \int_{\tau_0}^1 d\tau \int_{\tau}^1 \frac{dx_1}{x_1} \left[ u(x_1)u(x_2) + u(x_1)sea(x_2) + sea(x_1)u(x_2) \right. \\ & + d(x_1)d(x_2) + d(x_1)sea(x_2) + sea(x_1)d(x_2) \\ & \left. + 6sea(x_1)sea(x_2) \right] (\hat{\sigma} + \Delta\hat{\sigma})(\hat{s}), \end{aligned} \quad (14)$$

where  $\tau_0 = 4m_t^2/s$ ,  $x_2 = \tau/x_1$ ,  $\hat{s} = \tau s$ , and the parton distribution functions ( $u, d, sea$ ) are taken from Ref. [21] setting the scale  $Q = m_t$ .

---

<sup>3</sup>We thank C. Kao for point this out to us.

### 3 Numerical results

Inspecting the above formulas, one can immediately get an idea of the typical size of the one-loop corrections, as they are proportional to

$$\frac{\Delta\hat{\sigma}^{\text{EW}}}{\hat{\sigma}} \propto \left(\frac{\lambda_t}{4\pi}\right)^2, \quad \frac{\Delta\hat{\sigma}^{\text{QCD}}}{\hat{\sigma}} \propto \left(\frac{\alpha_s}{4\pi}\right). \quad (15)$$

For the favored values of  $m_t$ , both these factors are  $\sim 1\%$ . We thus see that unless there are enhancements within the loop factors contributing to these diagrams, both contributions are comparable in size, and more importantly, much too small to be disentangled from the Standard Model contribution, or to be observed experimentally at the Tevatron or any of its planned or proposed upgrades.

Dynamical enhancements are however possible for restricted ranges of the mass parameters. The top-quark self-energy diagrams show one such enhancement through the  $B'_0, B'_1$  functions when  $m_t \approx m_a + m_b$ , where  $m_{a,b}$  are the masses of the two particles entering the two-point function. The enhancement occurs right below the threshold for  $t \rightarrow a + b$  decay. For the top quark there are three possibilities for  $m_{a,b}$ :  $(m_{\tilde{t}_{1,2}}, m_{\chi_{1,2,3,4}^0})$ ;  $(m_{\tilde{t}_{1,2}}, m_{\chi_{1,2}^\pm})$ ; and  $(m_{\tilde{t}_{1,2}}, m_{\tilde{g}})$ . Given the present experimental lower limits on the squark (excluding  $\tilde{t}$ ) and gluino masses (*i.e.*,  $m_{\tilde{q}}, m_{\tilde{g}} > 175$  GeV;  $m_{\tilde{q}} \approx m_{\tilde{g}} > 230$  GeV [22]), only the first possibility may be realized. That is, enhancements may occur for  $m_t \approx m_{\tilde{t}_{1,2}} + m_{\chi_{1,2,3,4}^0}$ . Moreover, these enhancements will be maximized when the neutralinos have a high higgsino content. (We do not see such enhancements for the incoming part of the diagram because  $m_q \approx 0$ .)

In this region of parameter space (and for real values of  $N_{j4}$ ) one obtains the following approximate expression

$$\begin{aligned} \frac{\Delta\hat{\sigma}^{\text{EW}}}{\hat{\sigma}} &\approx \left(\frac{\lambda_t}{4\pi}\right)^2 \sum_{j=1}^4 (N_{j4})^2 \sum_{J=1}^2 2 \left[ m_t^2 B'_1 - (-1)^{J+1} \sin(2\theta_t) m_t m_{\chi_j^0} B'_0 \right] \\ &\rightarrow \left(\frac{\lambda_t}{4\pi}\right)^2 \sum_{J=1}^2 2 \left[ m_t^2 B'_1 - (-1)^{J+1} \sin(2\theta_t) m_t m_{\chi} B'_0 \right], \end{aligned} \quad (16)$$

where the second expression follows when one of the neutralinos ( $\chi$ ) carries the full higgsino admixture. Also, the choice  $\tan\beta = 1$  maximizes  $\lambda_t$  for a fixed value of  $m_t$ . In this ‘best case scenario’, one can plot  $\Delta\sigma/\sigma$  (*i.e.*, after integration over parton distribution functions) versus the neutralino mass ( $m_\chi$ ), and study the dependence on the top-squark masses and mixing angle. Note that the mixing-angle term does not contribute if the top-squark masses are degenerate.

In the case of degenerate masses, taken at  $m_{\tilde{t}_1} = m_{\tilde{t}_2} = 50$  (75) GeV, the resulting relative shift (%), as a function of  $m_\chi$ , is shown by the dotted curve on the upper-left-hand panel in Figs. 5 (6).<sup>4</sup> The large dips at  $m_\chi \approx m_t - m_{\tilde{t}_{1,2}} \approx$

---

<sup>4</sup>The numerical results in Figs. 5 and 6 have been obtained for the ‘best case scenario’ outlined below Eq. (16) and include the complete electroweak-like vertex and external leg corrections.

125 (100) GeV derive from the  $B'_1$  term in Eq. (16) and have been regularized by setting  $m_t^2 \rightarrow m_t^2 - im_t\Gamma_t$ , where  $\Gamma_t$  (a few GeV) is the top-quark decay width.<sup>5</sup> The depth of the dips depends on the value of  $m_\chi/m_t$  at which it occurs, and is maximized for  $m_\chi/m_t \approx 0.73$ , which in this case implies  $m_\chi \approx 128$  GeV,  $m_{\tilde{t}} \approx 47$  GeV (*i.e.*, as in Fig. 5 (dotted curve, upper-left-hand panel)).

In a more realistic scenario, light top-squarks cannot be degenerate in mass because limits on additional contributions to the  $\rho$  parameter restrict the splitting between the  $\tilde{t}_L$  and  $\tilde{b}_L \approx \tilde{b}_1$ , and from direct experimental searches one estimates that  $m_{\tilde{b}_1} > 200$  GeV. In the case of no top-squark mixing ( $\theta_t = 0, \frac{\pi}{2}$ ), the splitting of  $\tilde{t}_{1,2}$  leads to a double-dip structure if both top-squark masses are such that  $m_t \approx m_{\tilde{t}_{1,2}} + m_\chi$  can be satisfied, as in Fig. 5 (solid curve, upper-left-hand panel), where we have taken  $m_{\tilde{t}_1} = 50$  GeV and  $m_{\tilde{t}_2} = 100$  GeV. Note that the dips do not have the same depth, as discussed above. In Fig. 6 there is a single dip because we have taken  $m_{\tilde{t}_1} = 75$  GeV and  $m_{\tilde{t}_2} = 250$  GeV.

Yet more realistic is the case of top-squark mixing, which is naturally present in supergravity theories. This mixing tends to “screen” the contributions of top-squarks to the  $Z$ -pole observables [23], and therefore allows a larger  $\tilde{t}_L - \tilde{b}_L$  mass splitting. In Figs. 5 and 6 we present the results for four choices of the mixing angle  $\theta_t = 0, 0.10, 0.25$ , and maximal mixing ( $\frac{\pi}{4}$ ). The plots also apply for  $\theta_t \rightarrow \frac{\pi}{2} - \theta_t$ , which leaves  $\sin(2\theta_t)$  unchanged. In this case the  $B'_0$  function in Eq. (16) plays an important role, as it exhibits a similar dip behavior as  $B'_1$  does, although with a different sign at each dip. This effect makes one dip deeper (corresponding to  $\tilde{t}_1$ ) whereas the other one shallower (corresponding to  $\tilde{t}_2$ ), as evidenced in Fig. 5. The effect can be very significant, completely eliminating one of the dips at maximum mixing angle. In Fig. 6 only the dip that gets deeper exists.

As explained above, the QCD-like corrections are not expected to exhibit the dip structure that the electroweak-like corrections possess, because the relation  $m_t \approx m_{\tilde{g}} + m_{\tilde{t}}$  cannot be satisfied by the experimentally allowed gluino masses. In Fig. 7 we show the QCD-like correction versus the universal squark masses ( $m_{\tilde{t}_{1,2}} = m_{\tilde{q}}$ ) for fixed values of the gluino mass. The curve for  $m_{\tilde{g}} = 150$  GeV behaves differently from the others because for sufficiently light squark masses, the relation  $m_t \approx m_{\tilde{g}} + m_{\tilde{q}}$  will be satisfied, *i.e.*, a dip occurs. This region of parameter space is disfavored experimentally; it is shown here to make contact with Ref. [20], with which we agree qualitatively. From Fig. 7 we see that shifts as large as  $\sim 20\%$  may occur. We also observe that the corrections go to zero when the supersymmetric particle masses get large, *i.e.*, the expected decoupling effect. This figure also contains a curve (the dashed line) where all sparticle masses are taken to be the same ( $m_{\tilde{g}} = m_{\tilde{t}_{1,2}} = m_{\tilde{q}}$ ), which is seen to intercept the other curves at the appropriate places, and to decouple rather quickly.

The significant QCD-like shifts observed in Fig. 7, especially for  $m_{\tilde{g}} = 200$  GeV,

---

<sup>5</sup>Throughout our numerical calculations we have used  $m_t = 175$  GeV and  $m_t\Gamma_t = 289$  GeV<sup>2</sup>. For  $\alpha_s$  we took the world-average value of 0.118 at the scale  $\mu = M_Z$  in the modified minimal subtraction scheme.



may be understood in terms of the large color factor in the vertex correction diagrams that couple the gluon to two gluinos, both in the incoming (Fig. 3(c)) and outgoing (Fig. 3(g)) parts of the diagram. A relevant role may also be played by a dynamical enhancement of the vertex diagrams that occurs for  $\sqrt{\hat{s}} = 2m_{\tilde{g}}, 2m_{\tilde{q}}$ . As  $\sqrt{\hat{s}}$  is integrated over the parton distribution functions, starting at  $\sqrt{\hat{s}} = 2m_t$  and peaking at  $\sqrt{\hat{s}} \approx 400$  GeV, the typical cusp is smeared out but it appears visible as the peak in the dashed curve in Fig. 7 (obtained for  $m_{\tilde{q}} = m_{\tilde{g}}$ ).

In order to explore the effects of lighter top-squark masses, we concentrate on the  $m_{\tilde{q}} = m_{\tilde{g}}$  case<sup>6</sup> (the dashed line in Fig. 7) and in Fig. 8 we plot the QCD-like corrections for representative choices of  $(m_{\tilde{t}_1}, m_{\tilde{t}_2})$ . For reference, the all-equal-masses case is shown as a dashed line (as in Fig. 7). We can see that light top-squark masses enhance the corrections, especially in the region  $m_{\tilde{q}} = m_{\tilde{g}} \approx (200 - 250)$  GeV. This enhancement occurs (although to a lesser extent) even if only one of the top-squarks is light. We have also explored the effect of top-squark mixing, which is non-vanishing only if  $m_{\tilde{t}_1} \neq m_{\tilde{t}_2}$ . We find this effect to be rather small in the case of the QCD-like corrections amounting, for example, to a decrease in the peak value of the (50,250) curve in Fig. 8 by 15% for maximal mixing.

## 4 Expectations in specific models

The results presented in the previous section should represent the largest one-loop supersymmetric shifts (due to vertex and external leg corrections) to be expected in the top-quark cross section. However, in specific regions of MSSM parameter space or specific supergravity models, the shifts are likely to be much smaller than the largest possible ones, as the conditions for enhancement may not be satisfied: large electroweak-like shifts require a higgsino-like neutralino, light top-squarks,  $\tan\beta \approx 1$ , and a specific relation between their masses (*i.e.*,  $m_\chi + m_{\tilde{t}} \approx m_t$ ); large QCD-like shifts require  $m_{\tilde{q}}, m_{\tilde{g}} < 250$  GeV and light top-squarks. Interestingly enough, various scenarios (*i.e.*, selected regions of MSSM parameter space) recently proposed to possibly explain some experimental measurements that appear to deviate from Standard Model expectations, fall *precisely* in the class of models that may lead to one-loop enhancements of the top-quark cross section.

The discrepancy between the LEP measured value of  $R_b$  and its prediction in the Standard Model may be alleviated by supersymmetric loop corrections to the  $Zb\bar{b}$  vertex that involve charginos and top-squarks [9]. Moreover,  $\tan\beta$  should be close to 1, the charginos should be higgsino-like (and correspondingly the neutralinos too), and the top-squarks should be right-handed. Both should be as light as LEP 1.5 searches allow [24]. Since in this scenario there are no restrictions on the squark or gluino masses, let us concentrate on the electroweak-like corrections, that will be significantly enhanced (negatively) in this case if the relation  $m_\chi + m_{\tilde{t}} \approx m_t$  happens to be satisfied. This may indeed occur for  $m_{\tilde{t}_2}$  (but not for the desired values of  $m_{\tilde{t}_1}$

---

<sup>6</sup>The  $m_{\tilde{q}} \approx m_{\tilde{g}}$  relation occurs naturally in supergravity theories.

and  $m_\chi$ , both below  $M_W$ ).

In analogy with the so-called light-gluino window, it has been remarked that there is a light-higgsino window [10], where the Higgsino mixing parameter and the SU(2) gaugino mass are very small ( $\mu, M_2 \approx 0$ ) and  $\tan \beta \approx 1$ . In this scenario there are three neutralinos with significant higgsino admixtures, two with masses close to  $M_Z$  and a very light one. Moreover, a light top-squark is also desired to enhance  $R_b^{\text{susy}}$ . Therefore, if  $m_t \approx m_\chi + m_{\tilde{t}} \approx M_Z + m_{\tilde{t}}$  or equivalently  $m_{\tilde{t}} \approx m_t - M_Z \approx 85 \text{ GeV}$ , then the top-quark cross section will be shifted to lower values by a significant amount.

The last scenario we address has been advanced in Refs. [11, 12] as a possible explanation for the one much-publicized event at CDF, consisting of  $ee\gamma\gamma$  plus missing energy. This event has been ascribed to selectron pair-production, with decay into electron and second-to-lightest neutralino ( $\chi_2^0$ ), and further radiative decay of the neutralino into the LSP ( $\chi_2^0 \rightarrow \chi_1^0 + \gamma$ ). The missing energy is carried away by the pair of lightest neutralinos produced. The dominance of the (one-loop) radiative decay  $\chi_2^0 \rightarrow \chi_1^0 + \gamma$  over the more traditional ones ( $\chi_2^0 \rightarrow \chi_1^0 f \bar{f}$ ) provides the most important constraint on the parameter space, requiring a higgsino-like  $\chi_1^0$  and a photino-like  $\chi_2^0$ . This is achieved by setting the SU(2) and U(1) gaugino masses equal at the electroweak scale ( $M_1 = M_2$  and  $\tan \beta \approx 1$ ), precluding the gaugino mass unification in GUTs. Furthermore, the kinematics of the event appear to require:  $m_{\chi_1^0} \approx (30 - 55) \text{ GeV}$  and  $m_{\chi_2^0} \approx m_{\chi_1^0} + 30 \text{ GeV}$ . To make contact with the supersymmetric enhancement of  $R_b$ , it is also assumed that the top-squark is light ( $m_{\tilde{t}_1} \approx (45 - 60) \text{ GeV}$ ). In this case, however, the top-quark would have enhanced decays to  $\tilde{t} + \chi_1^0$ , thus diluting the observed top-quark sample. To undo this effect, it has been further proposed [12] that squarks and gluinos should be as light as experimentally allowed ( $m_{\tilde{g}} \approx (210 - 235) \text{ GeV}$ ,  $m_{\tilde{q}} \approx (220 - 250) \text{ GeV}$ ) such that  $\tilde{g} \rightarrow t\bar{t}$  decays add to the top-quark sample significantly. (This mechanism was originally proposed in Ref. [25].) Given these values of the squark and gluino masses, from Fig. 8 one can see that we generally expect  $\approx +15\%$  supersymmetric QCD-like corrections to the top-quark cross section. (There may also be significant electroweak-like corrections if  $m_{\tilde{t}_2} \approx m_t - m_{\chi_1^0} \approx (105 - 145) \text{ GeV}$ .)

Going beyond the specific models discussed above, the light top-squarks that enhance both electroweak-like and QCD-like corrections will likely decrease the canonical top-quark branching ratio into  $bW$  because of the availability of the supersymmetric decay channels  $t \rightarrow \tilde{t} + \chi$ . Indeed, the top-quark Yukawa coupling in Eq. (5) entails an enhanced coupling between the top-quark, a higgsino-like neutralino, and a right-handed top-squark. This situation is favored by the enhanced corrections discussed above, and therefore enhance the exotic decays of the top quark. At present there are no real experimental limits on  $B(t \rightarrow bW)$ , only on  $B(t \rightarrow bW)/B(t \rightarrow qW)$  [26]. The only limits on  $B(t \rightarrow bW)$  have been obtained by correlating the top-quark mass and cross section measurements with the Standard Model cross section, implying  $B(t \rightarrow \text{other}) < 25\%$  [27]. If the electroweak-like (negative) correction occurs when the exotic channel ( $t \rightarrow \tilde{t}\chi$ ) is kinematically allowed, the yield of  $bWbW$  events will be decreased by the two effects, implying an effective  $B(t \rightarrow bW)$  ratio as small as  $(0.65)(0.5) \approx 0.3$ , assuming a  $-35\%$  shift in the cross section and  $B(t \rightarrow \tilde{t}\chi) = 1/2$ .

However, we note that the enhancements to the electroweak-like corrections occur right *below* the threshold for top-quark decay into top-squark and neutralino (see Figs. 5,6), and therefore the exotic decay channel is effectively closed.

Recent complementary studies of top-quark properties in supersymmetric theories include supersymmetric one-loop corrections to the  $t \rightarrow \tilde{t}\chi$  exotic decay channel [28], supersymmetric three-body decays of the top quark [29], and one-loop supersymmetric corrections to the top-quark width [30].

## 5 Conclusions

The experimental study of the top quark has just begun in earnest, with its mass and cross section having been measured to some precision. The Main Injector upgrade of the Tevatron should essentially provide a top-quark factory, where observations will be confronted with theoretical expectations for cross sections and branching ratios. We have shown that these precise measurements may indeed point to deviations from the Standard Model, as may be expected in supersymmetric theories. These deviations may be quite sizeable and therefore easy to detect, especially in scenarios with rather light sparticles that have been proposed to explain various apparent experimental anomalies. In the longer term, the presence of top quarks at the LHC will constitute one of largest backgrounds in new physics searches. Therefore, it will be essential to have a very good understanding of top-quark physics beforehand, so that these backgrounds may be subtracted off appropriately.

## Acknowledgments

We would like to thank Jin Min Yang for useful discussions. R.R. would also like to thank Toby Falk, Craig Pryor and David Robertson for useful discussions. The work of J.K. and R.R. has been supported by the World Laboratory. The work of J. L. has been supported in part by DOE grant DE-FG05-93-ER-40717. The work of D.V.N. has been supported in part by DOE grant DE-FG05-91-ER-40633.

## Appendix

In this Appendix, we present analytical expressions for the one-loop supersymmetric electroweak-like vertex and external leg corrections to top-quark production by including all components of the neutralino (viz., the higgsino, the photino and the zino) and of the chargino (viz., the higgsino and the wino), as well as top-squark and bottom-squark mixing. Though the contributions are enhanced for higgsino-like neutralinos and charginos, in a detailed numerical calculation one would also need to include the contributions from gaugino-like neutralinos and charginos. We again ignore corrections arising from box diagrams.

The invariant amplitude for top-quark production via  $q\bar{q}$  annihilation can be written as

$$M = M_0 + \delta M \quad (17)$$

where  $M_0$  is the tree level amplitude and  $\delta M$  is the first-order electroweak-like correction.  $M_0$  and  $\delta M$  are given by

$$iM_0 = \bar{v}(p_2)(-ig_s T^A \gamma^\nu)u(p_1) \frac{-ig_{\nu\mu}}{\hat{s}} \bar{u}(p_3)(-ig_s T^A \gamma^\mu)v(p_4) \quad (18)$$

$$i\delta M = \bar{v}(p_2)(-ig_s T^A \gamma^\nu)u(p_1) \frac{-ig_{\nu\mu}}{\hat{s}} \bar{u}(p_3)\Lambda^\mu v(p_4) \quad (19)$$

where  $p_1, p_2, p_3$  and  $p_4$  are the incoming quark and anti-quark and outgoing top-quark and anti-top-quark momenta respectively.  $\Lambda^\mu$  can be written as

$$\Lambda^\mu = -ig_s T^A (F_1 \gamma^\mu + F_2 \gamma^\mu \gamma_5 + F_3 k^\mu + F_4 k^\mu \gamma_5 + F_5 i k_\nu \sigma^{\mu\nu} + F_6 i k_\nu \sigma^{\mu\nu} \gamma_5) \quad (20)$$

where  $k^\mu = p_1^\mu + p_2^\mu = p_3^\mu + p_4^\mu$  and  $\sigma^{\mu\nu} = \frac{i}{2}[\gamma^\mu, \gamma^\nu]$ . The form factors  $F_{1,\dots,5}$  encode the loop functions and depend on the various masses in the theory. The supersymmetric electroweak-like vertex and external leg corrections to the tree-level parton cross section are give by

$$\Delta\hat{\sigma}^{\text{EW}} = \frac{8\pi\alpha_s^2}{9\hat{s}^2} \beta_t \left[ \frac{2}{3}(\hat{s} + 2m_t^2)(F_1^n + F_1^c) + 2(F_5^n + F_5^c)m_t\hat{s} \right]. \quad (21)$$

We see that the corrections depend only on  $F_1$  and  $F_5$ . Below we present the complete form factors that appear in these equations. The tree-level parton cross section is given in Eq. (4).

The Feynman rules used to obtain the following form factors are given in Ref. [14]. For the electroweak-like corrections involving neutralinos and top-squarks we get

$$\begin{aligned} F_1^n = & \frac{1}{4\pi^2} \sum_{j=1}^4 \left\{ (|A_n \cos \theta_t + B_n \sin \theta_t|^2 + |C_n \cos \theta_t - A_n^* \sin \theta_t|^2) \right. \\ & \times \left[ c_{24} + m_t^2(c_{11} + c_{21}) + \frac{1}{2}B_1 + m_t^2 B_1' \right]^{(\chi_j^0, \tilde{t}_1, \tilde{t}_1)} \\ & \left. - \text{Re}[(A_n \cos \theta_t + B_n \sin \theta_t)(C_n^* \cos \theta_t - A_n \sin \theta_t)] 2m_t m_{\chi_j^0} (c_0 + c_{11} + B_0')^{(\chi_j^0, \tilde{t}_1, \tilde{t}_1)} \right\} \\ & + (\tilde{t}_1 \leftrightarrow \tilde{t}_2, \cos \theta_t \leftrightarrow -\sin \theta_t, \sin \theta_t \leftrightarrow \cos \theta_t); \end{aligned} \quad (22)$$

$$\begin{aligned} F_5^n = & \frac{1}{4\pi^2} \sum_{j=1}^4 \left\{ (|A_n \cos \theta_t + B_n \sin \theta_t|^2 + |C_n \cos \theta_t - A_n^* \sin \theta_t|^2) \left[ -\frac{1}{2}m_t(c_{11} + c_{21}) \right]^{(\chi_j^0, \tilde{t}_1, \tilde{t}_1)} \right. \\ & \left. + \text{Re}[(A_n \cos \theta_t + B_n \sin \theta_t)(C_n^* \cos \theta_t - A_n \sin \theta_t)] m_{\chi_j^0} (c_0 + c_{11})^{(\chi_j^0, \tilde{t}_1, \tilde{t}_1)} \right\} \\ & + (\tilde{t}_1 \leftrightarrow \tilde{t}_2, \cos \theta_t \leftrightarrow -\sin \theta_t, \sin \theta_t \leftrightarrow \cos \theta_t), \end{aligned} \quad (23)$$

where (in the notation of Ref. [14])

$$A_n = -\frac{i}{2} \frac{gm_t}{\sqrt{2}M_W \sin \beta} N_{j4}^* = -\frac{i}{2} \lambda_t N_{j4}^* \quad (24)$$

$$B_n = \frac{i}{\sqrt{2}} \left[ \frac{2}{3} e N_{j1}^* - \frac{2 \sin^2 \theta_W}{3 \cos \theta_W} g N_{j2}^* \right] \quad (25)$$

$$C_n = -\frac{i}{\sqrt{2}} \left[ \frac{2}{3} e N_{j1}' - \frac{2 \sin^2 \theta_W}{3 \cos \theta_W} g N_{j2}' + \frac{1}{2 \cos \theta_W} g N_{j2}' \right] \quad (26)$$

Recall also that  $\tilde{t}_1 = \cos \theta_t \tilde{t}_L + \sin \theta_t \tilde{t}_R$  and  $\tilde{t}_2 = -\sin \theta_t \tilde{t}_L + \cos \theta_t \tilde{t}_R$ . The various  $B$  and  $c$  functions in the above expressions are the well documented Passarino-Veltman functions [15] (adapted to our metric where  $p_i^2 = m_i^2$ ); the  $B$  functions depend on  $(m_t, m_{\chi_j^0}, m_{\tilde{t}_{1,2}})$  whereas the  $c$  functions depend on  $(-p_3, p_3 + p_4, m_{\chi_j^0}, m_{\tilde{t}_{1,2}}, m_{\tilde{t}_{1,2}})$  [as reminded by the superscripts in Eqs. (22,23)]. We note that in the expressions for  $F_{1,5}^n$  given in the main text in Eqs. (7,8), which are specific to the case  $N_{j1}' = N_{j2}' = 0$ , we have extracted an overall factor of  $(\lambda_t/4\pi)^2$ .

The form factors for the electroweak-like corrections due to loops involving charginos and bottom-squarks are given by

$$\begin{aligned} F_1^c &= \frac{1}{4\pi^2} \sum_{j=1}^2 \left\{ (|A_c \cos \theta_b|^2 + |B_c \cos \theta_b + C_c \sin \theta_b|^2) \right. \\ &\quad \times \left[ c_{24} + m_t^2 (c_{11} + c_{21}) + \frac{1}{2} B_1 + m_t^2 B_1' \right]^{(\chi_j^\pm, \tilde{b}_1, \tilde{b}_1)} \\ &\quad \left. - \text{Re} [A_c \cos \theta_b (B_c^* \cos \theta_b + C_c^* \sin \theta_b)] 2m_t m_{\chi_j^\pm} (c_0 + c_{11} + B_0')^{(\chi_j^\pm, \tilde{b}_1, \tilde{b}_1)} \right\} \\ &\quad + (\tilde{b}_1 \leftrightarrow \tilde{b}_2, \cos \theta_b \leftrightarrow -\sin \theta_b, \sin \theta_b \leftrightarrow \cos \theta_b) ; \end{aligned} \quad (27)$$

$$\begin{aligned} F_5^c &= \frac{1}{4\pi^2} \sum_{j=1}^2 \left\{ (|A_c \cos \theta_b|^2 + |B_c \cos \theta_b + C_c \sin \theta_b|^2) \left[ -\frac{1}{2} m_t (c_{11} + c_{21}) \right]^{(\chi_j^\pm, \tilde{b}_1, \tilde{b}_1)} \right. \\ &\quad \left. + \text{Re} [A_c \cos \theta_b (B_c^* \cos \theta_b + C_c^* \sin \theta_b)] m_{\chi_j^\pm} (c_0 + c_{11})^{(\chi_j^\pm, \tilde{b}_1, \tilde{b}_1)} \right\} \\ &\quad + (\tilde{b}_1 \leftrightarrow \tilde{b}_2, \cos \theta_b \leftrightarrow -\sin \theta_b, \sin \theta_b \leftrightarrow \cos \theta_b) , \end{aligned} \quad (28)$$

where (in the notation of Ref. [14])

$$A_c = \frac{i}{2} \frac{gm_t}{\sqrt{2}M_W \sin \beta} V_{j2}^* = \frac{i}{2} \lambda_t V_{j2}^* \quad (29)$$

$$B_c = -\frac{i}{2} g U_{j1} \quad (30)$$

$$C_c = \frac{i}{2} \frac{gm_b}{\sqrt{2}M_W \cos \beta} U_{j2} = \frac{i}{2} \lambda_b U_{j2} . \quad (31)$$

Also,  $\theta_b$  is the bottom-squark mixing angle defined such that  $\tilde{b}_1 = \cos \theta_b \tilde{b}_L + \sin \theta_b \tilde{b}_R$  and  $\tilde{b}_2 = -\sin \theta_b \tilde{b}_L + \cos \theta_b \tilde{b}_R$ . In this case the  $B$  functions depend on  $(m_t, m_{\chi_j^\pm}, m_{\tilde{b}_{1,2}})$

whereas the  $c$  functions depend on  $(-p_3, p_3 + p_4, m_{\chi_j^\pm}, m_{\tilde{b}_{1,2}}, m_{\tilde{b}_{1,2}})$ . Note also that in the expressions for  $F_{1,5}^c$  given in the main text in Eqs. (9,10), which are specific to the case  $U_{j1} = U_{j2} = 0$ , we have extracted an overall factor of  $(\lambda_t/4\pi)^2$ .

## References

- [1] CDF Collaboration, F. Abe et al., Phys. Rev. Lett. **74** (1995) 2676; D0 Collaboration, S. Abachi et al., Phys. Rev. Lett. **74** (1995) 2632.
- [2] A. Caner (CDF Collaboration), presented at the 1996 La Thuile Conference; M. Narain (D0 Collaboration), presented at the 1996 La Thuile Conference.
- [3] “Future ElectroWeak Physics at the Fermilab Tevatron”, Report of the TeV 2000 Working Group, FERMILAB-PUB-96/082, edited by D. Amidei and R. Brock.
- [4] E. Laenen, J. Smith, and W. van Neerven, Nucl. Phys. B **369** (1992) 543 and Phys. Lett. B **321** (1994) 254.
- [5] E. Berger and H. Contopanagos, Phys. Lett. B **361** (1995) 115 and hep-ph/9603326.
- [6] S. Catani, M. Mangano, P. Nason, and L. Trentadue, hep-ph/9602208.
- [7] J. Yang and C. Li, Phys. Rev. D **52** (1995) 1541.
- [8] C. Li, B. Hu, J. Yang, and C. Hu, Phys. Rev. D **52** (1995) 5014.
- [9] J. D. Wells, C. Kolda, and G. L. Kane, Phys. Lett. B **338** (1994) 219; D. Garcia, R. Jimenez, and J. Sola, Phys. Lett. B **347** (1995) 321; D. Garcia and J. Sola, Phys. Lett. B **357** (1995) 349; X. Wang, J. L. Lopez, and D. V. Nanopoulos, Phys. Rev. D **52** (1995) 4116; J. Wells and G. Kane, Phys. Rev. Lett. **76** (1996) 869; J. Ellis, J. L. Lopez, and, D. V. Nanopoulos, Phys. Lett. B **372** (1996) 95; A. Brignole, F. Feruglio, and F. Zwirner, hep-ph/9601293; P. Bamert, *et. al.*, hep-ph/9602438; P. Chankowski and S. Pokorski, hep-ph/9603310.
- [10] J. Feng, N. Polonsky, and S. Thomas, Phys. Lett. B **370** (1996) 95.
- [11] S. Ambrosanio, G. Kane, G. Kribs, S. Martin, and S. Mrenna, Phys. Rev. Lett. **76** (1996) 3498; S. Dimopoulos, M. Dine, S. Raby, and S. Thomas, Phys. Rev. Lett. **76** (1996) 3502; G. Kane and J. Wells, hep-ph/9603336.
- [12] G. Kane and S. Mrenna, hep-ph/9605351.
- [13] S. Park, in Proceedings of the 10th Topical Workshop on Proton-Antiproton Collider Physics, Fermilab, 1995, edited by R. Raja and J. Yoh (AIP, New York, 1995), p. 62.

- [14] H. Haber and G. Kane, Phys. Rep. **117** (1985) 75; J. Gunion and H. Haber, Nucl. Phys. B **272** (1986) 1 and Nucl. Phys. B **402** (1993) 567 (erratum).
- [15] G. Passarino and M. Veltman, Nucl. Phys. B **160** (1979) 151.
- [16] G.J. van Oldenborgh and J.A.M. Vermaseren, Z. Phys. C**46** (1990) 425.
- [17] J. Yang and C. Li, erratum to Ref. [7] (to appear).
- [18] J. Yang and C. Li, hep-ph/9603442.
- [19] J. Ellis and D. Ross, hep-ph/9604432. See also, P. Kraus and F. Wilczek, hep-ph/9601279.
- [20] C. Li, B. Hu, J. Yang, and C. Hu, Phys. Rev. D **53** (1996) 4112.
- [21] J. Morfin and. W. Tung, Z. Phys. C**52** (1991) 13.
- [22] S. Abachi, *et. al.* (D0 Collaboration), Phys. Rev. Lett. **75** (1995) 618; F. Abe, *et. al.* (CDF Collaboration), Phys. Rev. Lett. **69** (1992) 3439 and Phys. Rev. Lett. **76** (1996) 2006; J. Hauser, in Proceedings of the 10th Topical Workshop on Proton-Antiproton Collider Physics, Fermilab, 1995, edited by R. Raja and J. Yoh (AIP, New York, 1995), p. 13.
- [23] A. Dabelstein, W. Hollik, and W. Mosle, hep-ph/9506251 and references therein.
- [24] D. Buskulic, *et. al.* (ALEPH Collaboration), Phys. Lett. B **373** (1996) 24; L. Dijkstra (DELPHI Collaboration), CERN-PPE-95-004; M. Acciarri, *et. al.* (L3 Collaboration), CERN-PPE-96-029; G. Alexander, *et. al.* (OPAL Collaboration), CERN-PPE-96-020.
- [25] T. Kon and T. Nonaka, Phys. Rev. D **50** (1994) 6005.
- [26] J. Incandela (CDF Collaboration), FERMILAB-CONF-95-237-E (July 1995); T. LeCompte (CDF Collaboration), FERMILAB-CONF-96/021-E (January 1996).
- [27] X. Wang, J. L. Lopez, and D. V. Nanopoulos, in Ref. [9]; S. Mrenna and C. P. Yuan, Phys. Lett. B **367** (1996) 188.
- [28] A. Djouadi, W. Hollik, and C. Junger, hep-ph/9605340.
- [29] J. Guasch and J. Sola, hep-ph/9603441.
- [30] J. Sola, hep-ph/9605306.

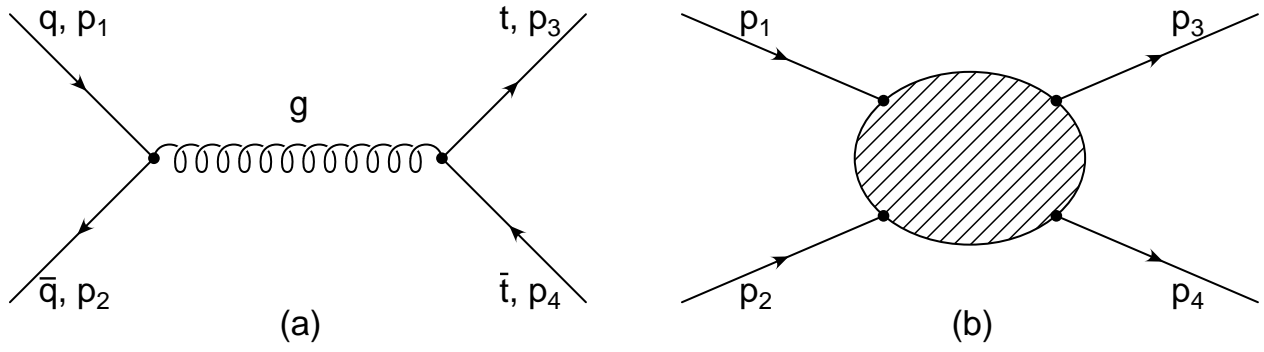


Figure 1: Tree-level diagram (a) describing  $q\bar{q} \rightarrow t\bar{t}$  production. The blob diagram (b) indicates the choice of external momenta used throughout our calculations.



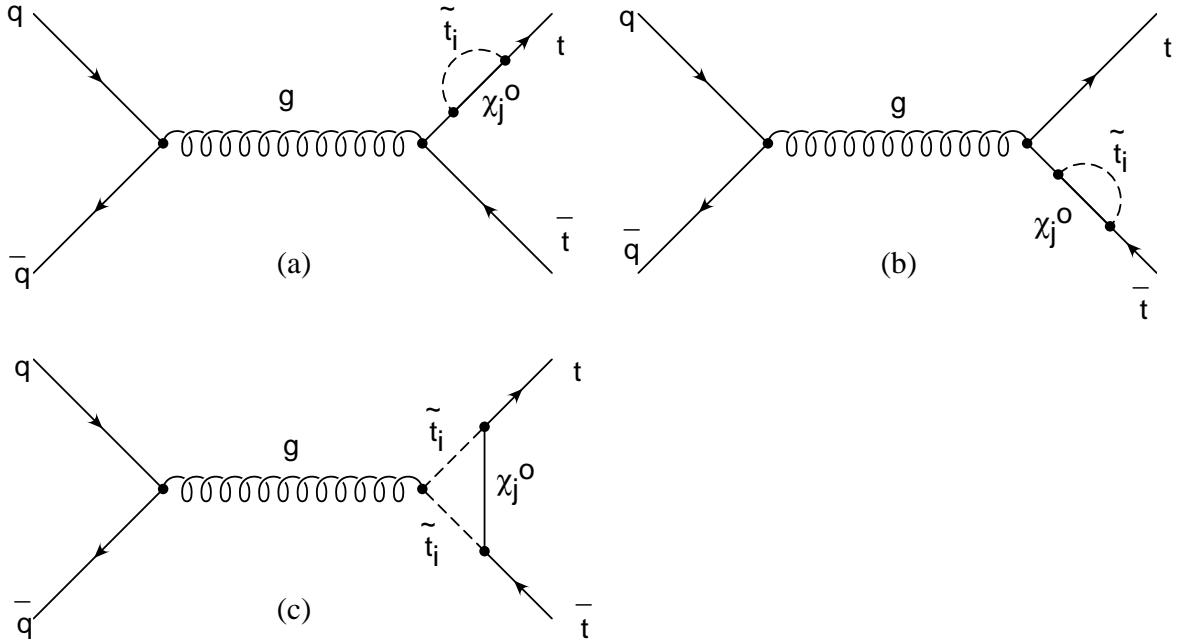


Figure 2: Feynman diagrams describing the one-loop supersymmetric electroweak-like corrections to  $q\bar{q} \rightarrow t\bar{t}$ , including external leg corrections (a,b) and vertex corrections (c) from top-squark and neutralino loops. An analogous set of diagrams exists where the top-squarks are replaced by bottom-squarks and the neutralinos by charginos.

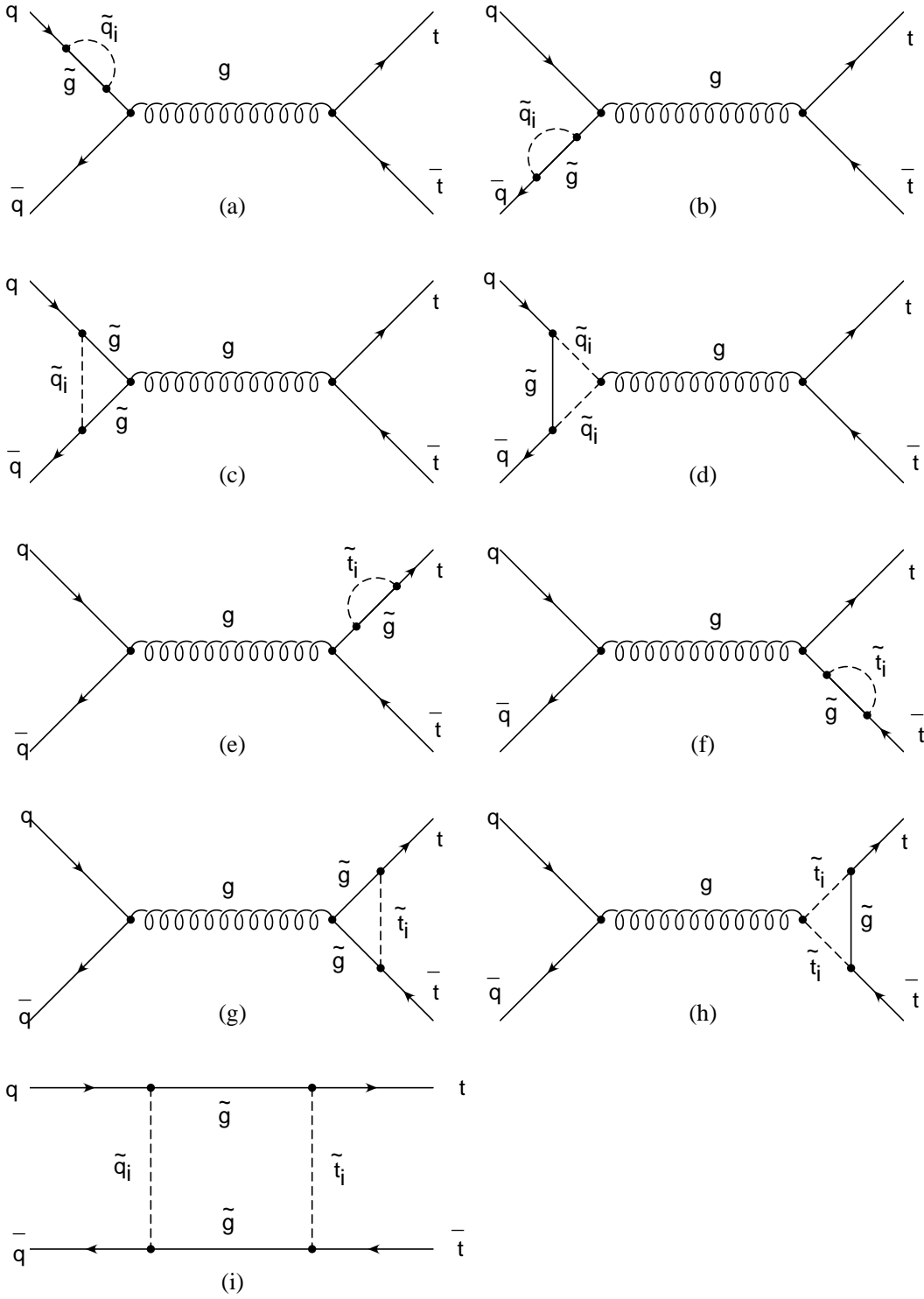


Figure 3: Feynman diagrams describing the one-loop supersymmetric QCD-like corrections to  $q\bar{q} \rightarrow t\bar{t}$ , including external leg corrections (a,b,e,f), vertex corrections (c,d,g,h), and a representative box diagram (i).

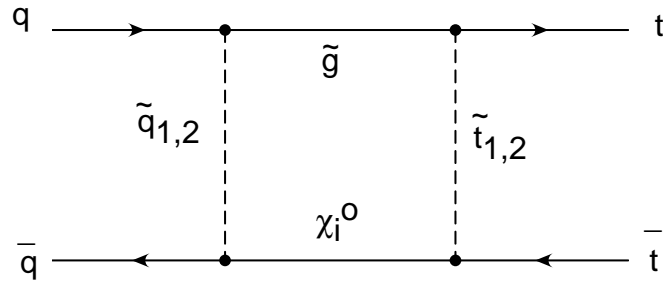


Figure 4: Representative box diagram (one of four possible ones) describing the mixed one-loop supersymmetric QCD-like and electroweak-like corrections.

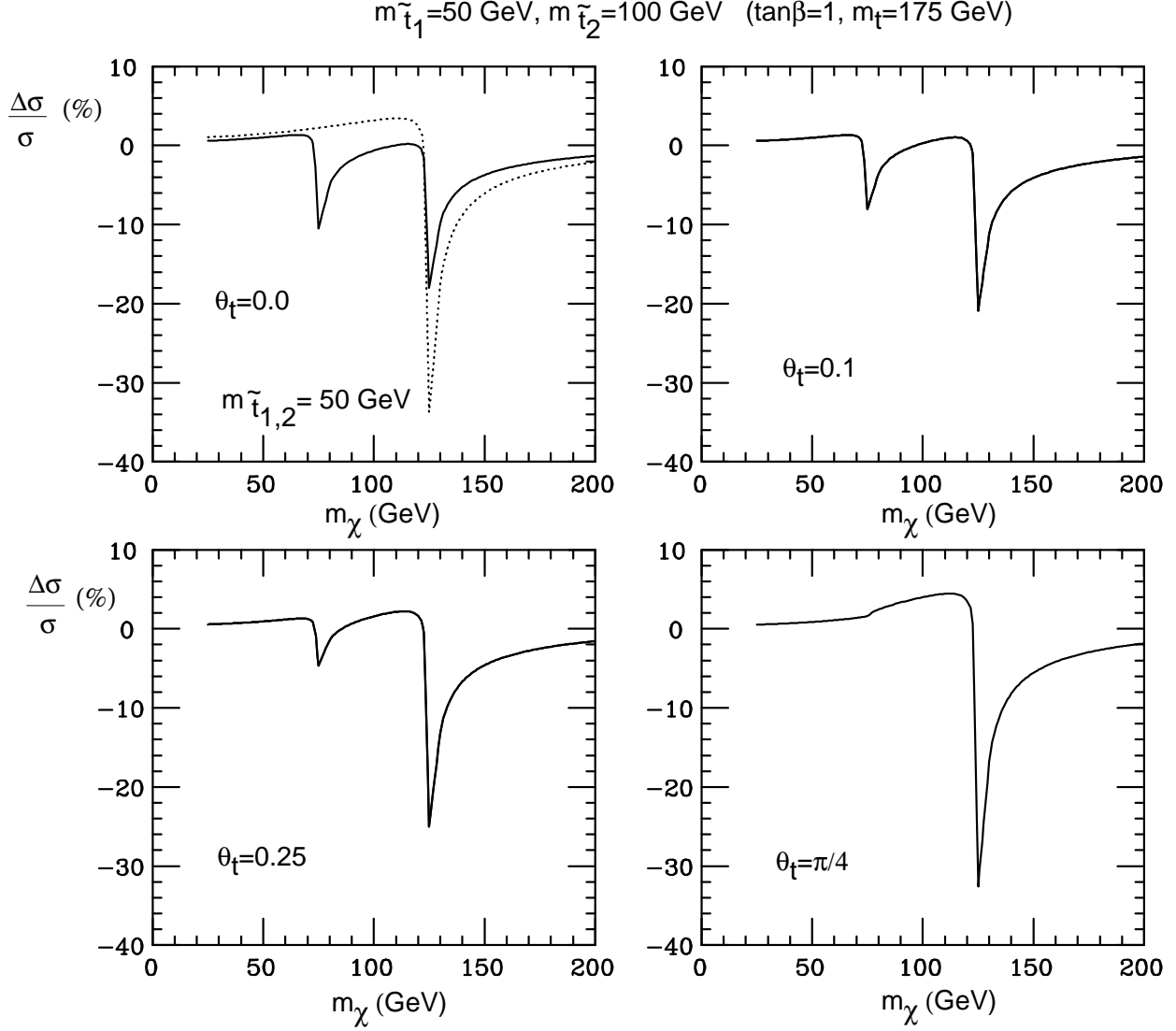


Figure 5: The relative (%) one-loop supersymmetric electroweak-like correction to the top-quark pair-production cross section at the Tevatron as a function of the (higgsino-like) neutralino mass, for  $m_t = 175 \text{ GeV}$ ,  $\tan\beta = 1$ ,  $m_{\tilde{t}_1} = 50 \text{ GeV}$ ,  $m_{\tilde{t}_2} = 100 \text{ GeV}$ , and various choices of the top-squark mixing angle ( $\theta_t = 0.0, 0.10, 0.25, \frac{\pi}{4}$ ). The dotted curve on the upper-left-hand panel corresponds to  $m_{\tilde{t}_1} = m_{\tilde{t}_2} = 50 \text{ GeV}$ . Note the dips on the curves when  $m_t \approx m_{\tilde{t}_{1,2}} + m_\chi$ .

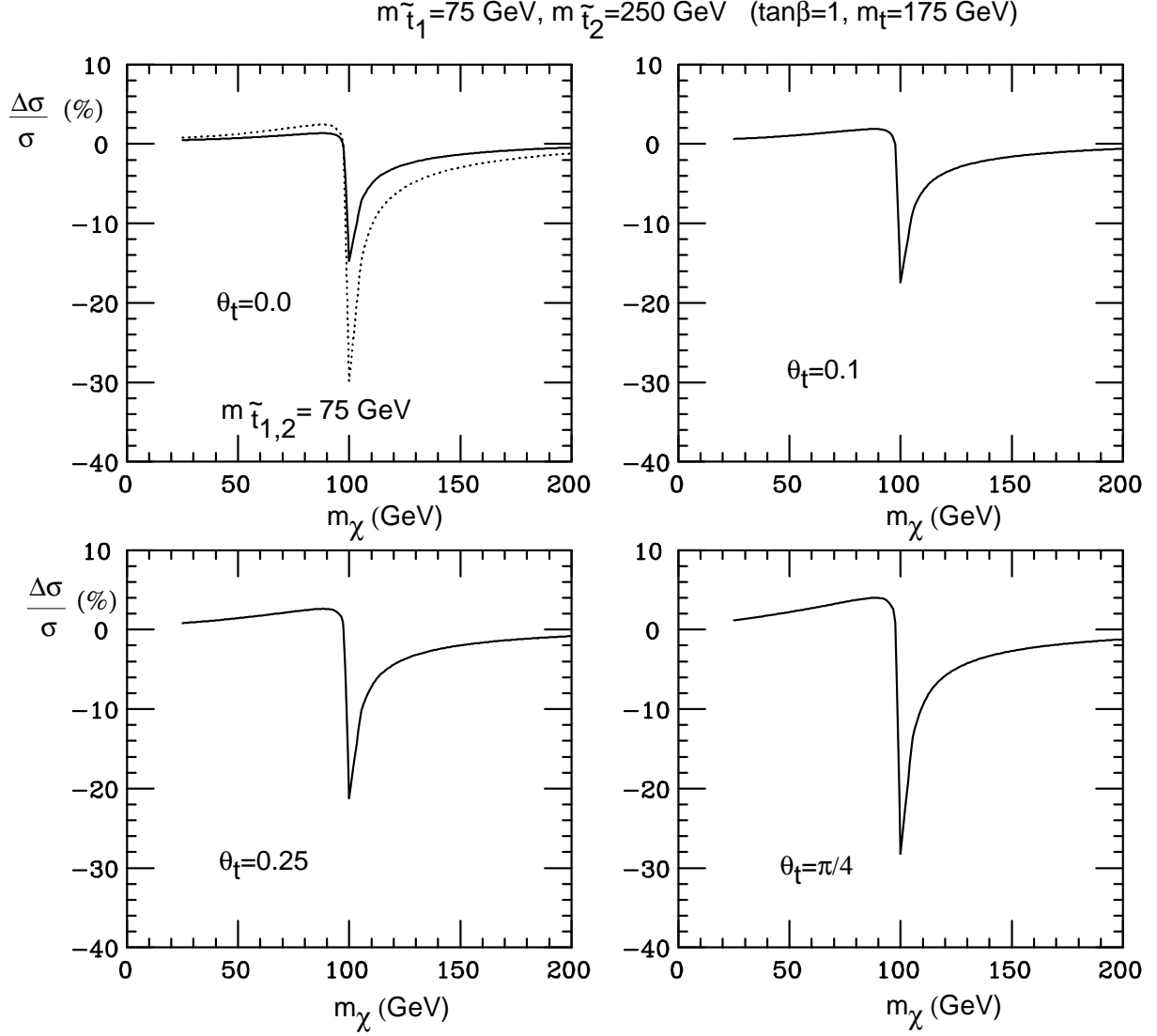


Figure 6: The relative (%) one-loop supersymmetric electroweak-like correction to the top-quark pair-production cross section at the Tevatron as a function of the (higgsino-like) neutralino mass, for  $m_t = 175 \text{ GeV}$ ,  $\tan\beta = 1$ ,  $m_{\tilde{t}_1} = 75 \text{ GeV}$ ,  $m_{\tilde{t}_2} = 250 \text{ GeV}$ , and various choices of the top-squark mixing angle ( $\theta_t = 0.0, 0.10, 0.25, \frac{\pi}{4}$ ). The dotted curve on the upper-left-hand panel corresponds to  $m_{\tilde{t}_1} = m_{\tilde{t}_2} = 75 \text{ GeV}$ . Note the dips on the curves when  $m_t \approx m_{\tilde{t}_{1,2}} + m_\chi$ .

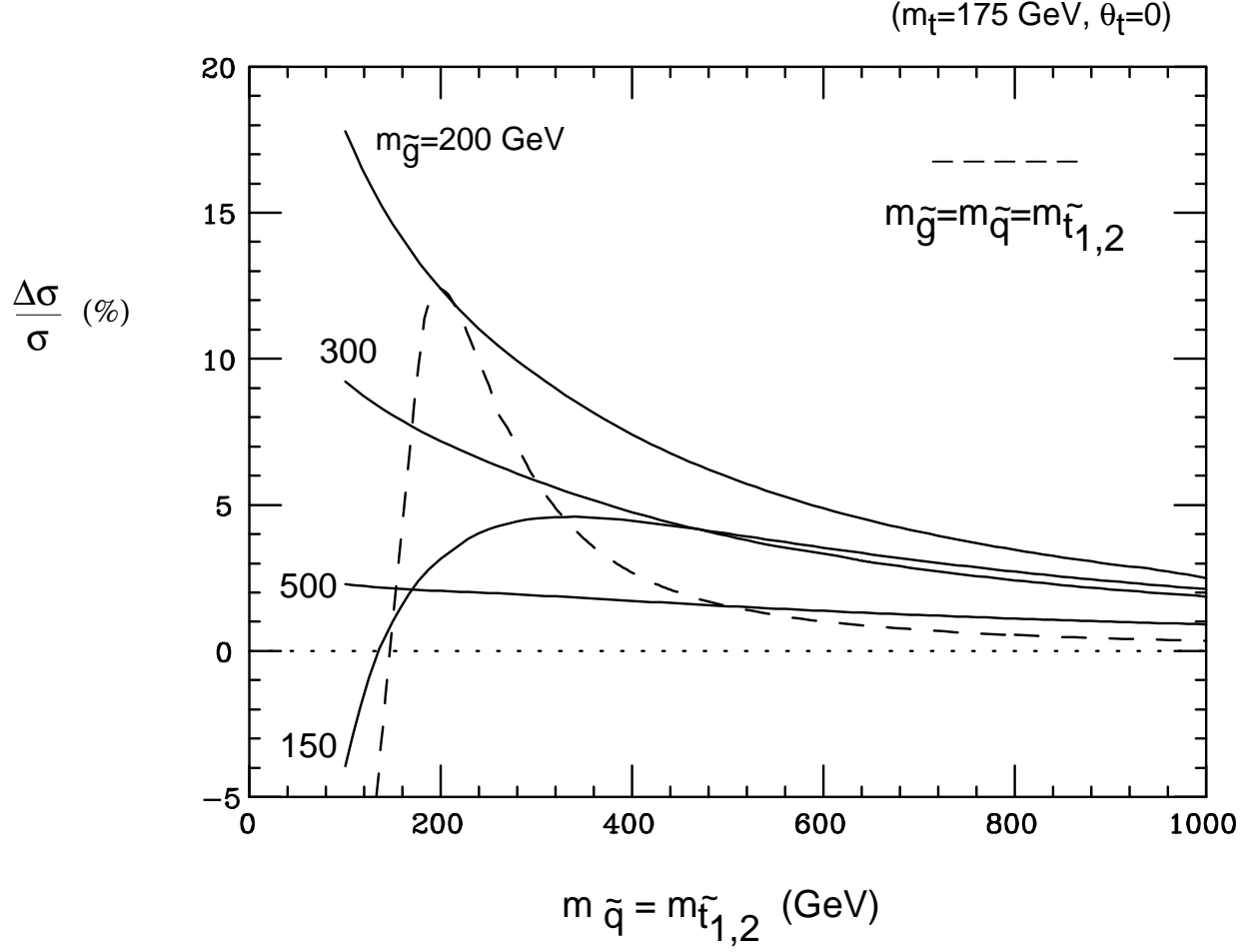


Figure 7: The relative (%) one-loop supersymmetric QCD-like correction to the top-quark pair-production cross section at the Tevatron as a function of the universal squark mass, for  $m_t = 175$  GeV and the indicated choices of the gluino mass. The dashed curve represents the  $m_{\tilde{g}} = m_{\tilde{q}}$  case.

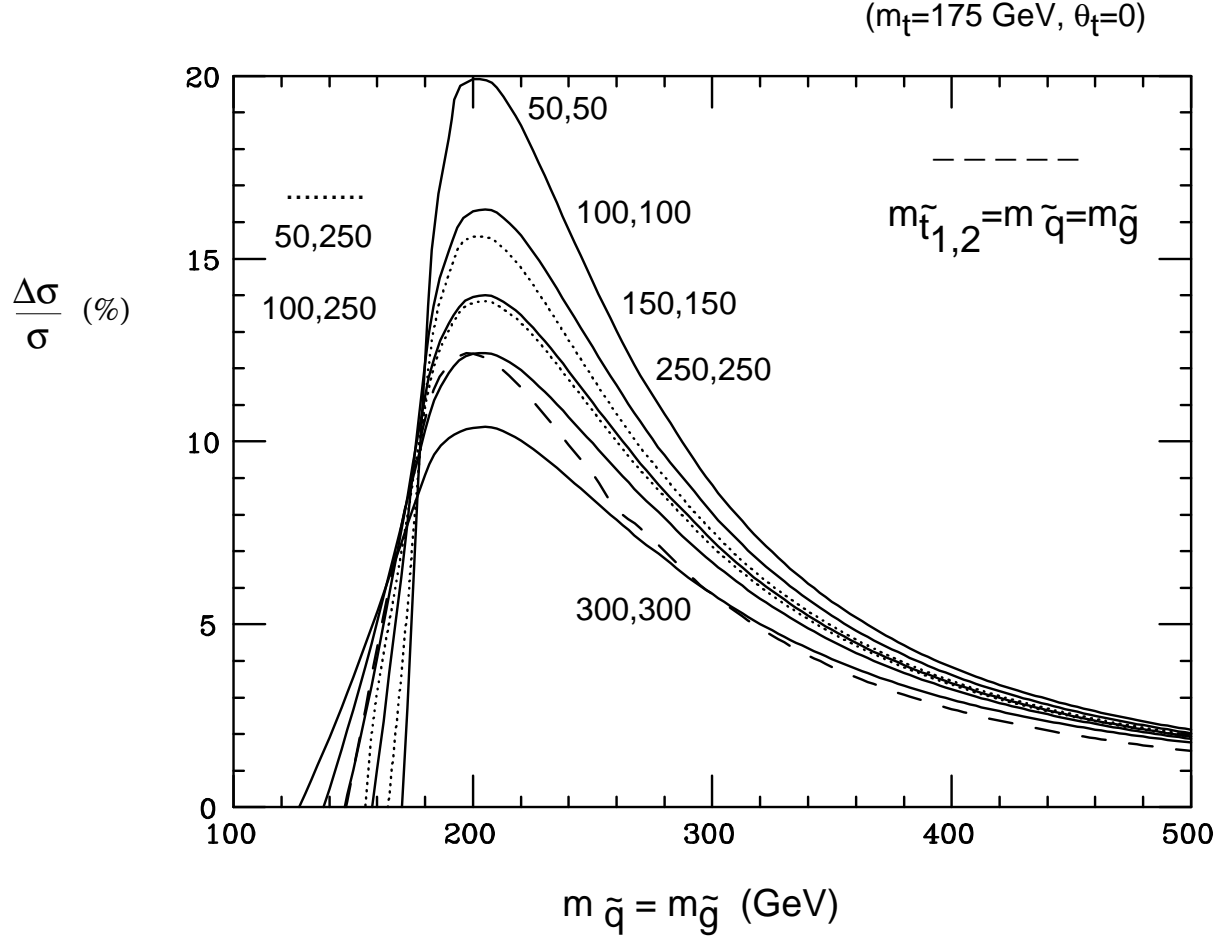


Figure 8: The relative (%) one-loop supersymmetric QCD-like correction to the top-quark pair-production cross section at the Tevatron as a function of the squark or gluino mass, for  $m_t = 175$  GeV and for the indicated choices of top-squark masses  $(m_{\tilde{t}_1}, m_{\tilde{t}_2})$ . The dotted curves highlight the effect of non-degenerate top-squark masses. The dashed curve represents the fully degenerate  $m_{\tilde{t}_{1,2}} = m_{\tilde{g}} = m_{\tilde{q}}$  case.